DR2011047

Faulted terrace risers place new constraints on the late Quaternary slip rate for the central Altyn Tagh Fault, northwest Tibet

Authors: Ryan D. Gold[1†], Eric Cowgill[1], J Ramón Arrowsmith[2], Xuanhua Chen[3], Warren D. Sharp[4], Kari M. Cooper[1], Xiao-Feng Wang[3]

[1]Department of Geology, University of California, Davis, CA 95616, U.S.A.
[2]School of Earth and Space Exploration, Arizona State University, Tempe, AZ 85287, U.S.A
[3]Institute of Geomechanics, Chinese Academy of Geological Sciences, Beijing 100081, P. R. China
[4]Berkeley Geochronology Center, Berkeley, CA, 94709
[†]*now at* Geologic Hazards Science Center, U.S. Geological Survey, Denver, CO 80225

Summary

The supplemental material contains 7 sections. We begin with a description of our survey and mapping methods (DR1). Next, we report additional information regarding the ^{14}C analyses, including a summary of analytical methods (DR2) and detailed discussions of results from Kelutelage (DR3) and Yukuang (DR4). We conclude with a discussion of the Keke Qiapu site (DR5) and the samples and methods applied at the site including U-series (DR6) and TCN dating (DR7). In addition, the supplemental data contains supporting figures with remotely sensed imagery, uninterpreted DTMs, and results from Keke Qiapu (Figures DR1-DR11). Lastly, tables are provided with ^{14}C results from Kelutelage (Table DR1) and Yukuang (Table DR2) as well as the U-series (Table DR3) and TCN (Table DR4) results from Keke Qiapu.

DR1. Survey Methods

We made observations at Kelutelage, Yukuang, and Keke Qiapu in 2005, 2006, and 2007. We followed the surveying protocol described by Gold et al. (2009), where a Leica

TCR407power total station was used to measure the boundaries of landforms such as the edges of the fault zone and riser crests and to generate coarse topographic constraints (3-5 m point spacing). Additionally, at the Kelutelage site we augmented the topographic survey by using a Trimble GX DR200+ Terrestrial Light Detection And Ranging unit (T-LiDAR). Map orientations at all three sites were determined using a handheld Brunton compass. We estimate the external accuracy of trends (world coordinate system) to be better than 5°. The internal precision of the survey projects is estimated to be sub-4 cm in both horizontal and vertical directions (e.g., Gold et al., 2009). Thus internally, reported trends are estimated to be better than 1°, which is a much higher level of precision than the geologic variability and ambiguity of the location of contacts.

At Kelutelage, we made 3232 topographic point measurements with the total station and we measured the positions of control points, which consisted of 1-m-long rebar rods pounded into the ground at prominently visible points throughout the site. These control points were also measured using the laser scanner to enable co-registration of the neotectonic mapping and LiDAR-derived digital terrain model (DTM). We used the T-LiDAR scanner to make a topographic survey of the site with an average point density of ~320 points/m^2. The laser scanner survey included 5 stations, covering an area of 280 x 320 m (E-W x N-S) with ~28.5 million topographic points. At each scan station, we measured the position of 4-6 targets set up over control points. The scans were co-registered using the control points with RealWorksSurvey version 6.1.2. The internal precision of the merged, raw point cloud dataset is estimated to be better than 4 cm in the horizontal and vertical (Gold et al., 2009). The topography presented in Figure 5 (main text) was generated by decimating the original T-LiDAR dataset to ~1.7 million topographic points and then applying an Ordinary Kriging algorithm (e.g., Dubrule, 1983) to generate a 0.3 m cell sized DTM using the Spatial Analyst extension in ArcGIS 9.2.

At Yukuang, we made 10,345 topographic point measurements with the total station with an average point density of ~0.14 points/m^2 covering an area of 300 m x 240 m (E-W x N-S). At Keke Qiapu, we made 5101 topographic point measurements with the total station with an average point density of ~0.13 points/m^2 covering an area of 170 m x 230 m (E-W x N-S). The internal precision of the Yukuang and Keke Qiapu topographic datasets is estimated to be better than 2 cm in the horizontal and vertical.

DR2. Radiocarbon (^{14}C) methods

We categorized organic samples for ^{14}C based on field observations and subsequent examination under a binocular microscope in the laboratory. The woody plant fragments consisted of wood-grained strands of light-to-dark brown materials ranging in length from 1-8 cm and in diameter from 0.1-2.0 cm. The root fragments consisted of morphologies similar to the woody fragments, but tended to be more tubular and were sometimes noted to connect with networks of anastomosing woody plant material. The animal fur specimen consisted of supple, light-brown, straw-like strands 4-6 cm in length. At Yukuang, the charcoal specimens were dark gray and dull in luster.

We followed the sampling and laboratory protocols previously described by Cowgill et al. (2009) and Gold et al. (2009). As with samples at Tuzidun (2009), plant materials deposited during terrace and loess deposition were often difficult to distinguish from roots which grew at the site at a time post-dating formation of the offset risers. We use the age patterns along with field observations and photographs to discriminate modern samples from those specimens with ages relating to the formation of the geomorphic features. The samples were analyzed via accelerator mass spectrometry (AMS) and the ^{14}C ages were calibrated using InterCal04 (Reimer et al., 2004) with the calibration software OxCal v.4.0.1 (Bronk Ramsey, 1995, 2001). For those ^{14}C ages with a 2-sigma (2-σ) uncertainty that is <0.1 ka, we assign an uncertainty of 0.1 ka in the landform age assessments to account for detrital age signals.

DR3. Radiocarbon (^{14}C) results from Kelutelage

Radiocarbon data from Kelutelage are here presented, beginning with the samples extracted from trenches excavated into F3 and F2 at the crest and base of the F3/F2 riser, respectively, and then from trenches excavated into F2 and F1 at the crest and base of the F2/F1 riser, respectively (Table DR1). We analyzed 6 samples from two trenches excavated into the F3 terrace deposit (Figure 8, main text). 4 samples were extracted from trench T3NE-A, above the upstream F3/F2 riser and 2 samples were collected from the T3SE-A trench, above the correlative, downstream F3/F2 riser segment. The oldest samples, C-48, C-49, and C-50 (8.2-14.4 ka) were collected from within the lowermost unit observed within the F3 terrace deposit and they are interpreted to be detrital, though they may also record the age of the deeper F3 deposit. A younger sample, C-47 (6.6 ± 0.1 ka), was collected from the overlying upper F3 deposit. From the downstream, T3SE-A trench, samples C-51 (5.7 ± 0.1 ka) and C-52 (6.2 ± 0.1 ka) were collected from within the F3 terrace deposit. We noted that sample C-51 might be a root, based on its woody morphology and its association with a continuous seam of plant material. On the basis of this field observation, as well as comparison of the young age, relative to samples from the cross-fault F3 deposit and to the lower and younger F2 surface, which are also older than C-51, we think that it is most likely that this sample is a root which grew into the F3 terrace deposit following F3 abandonment.

We analyzed 19 samples from two trenches excavated into the F2 deposit at the base of the F3/F2 riser face (Figure 8, main text). From trench T2NE-B, 6 samples were extracted from the colluvial material covering the riser face and 4 samples were collected from the underlying F2 terrace. The samples span the interval from 5.6-6.2 ka. None of the samples reflect age or characteristics, which would suggest either a detrital or root signal. From trench T2SE-B south of the fault, 6 samples were extracted from the colluvial material covering the riser face and 3 from the underlying F2 terrace. The samples from within the terrace (C-44, C-45, and C-46) range in age from 5.4-6.1 ka. The stratigraphically highest sample, C-44 (5.8 ± 0.1 ka), was sampled at the loess/tread contact. From the overlying loess, the oldest sample was C-43 (5.1 ± 0.2 ka). The morphology of the additional 5 samples collected from the loess wedge range in age from 1.1-2.2 ka. These samples were tubular and woody and they connected with extensive root networks within the loess wedge. This morphology is consistent with an interpretation that they were roots, which grew into the loess wedge following deposition of the loess material.

We analyzed 10 samples (1 replicate analysis, samples C-33 and C-34) from two trenches excavated into the F2 terrace at the crest of the F2/F1 riser (Figure 8, main text). Trench T2NE-A was excavated north of the fault. From this trench, 4 non-modern samples excavated from within the F2 terrace range in age from 4.0-6.5 ka. The remaining sample, C-21, yielded a modern age. From the crest of the downstream F2/F1 riser segment, we analyzed five unique samples from the F2 terrace collected from the T2SE-A trench. Samples C-32, C-33, C-34, C-36, and C-37 cluster from 5.7-6.1 ka. No distinguishable stratigraphic/age pattern exists within these samples. Sample C-35 yielded an anomalously old age of 26.5 ± 3.3 ka. This fragile charcoal sample was black and soft and exhibited a block morphology with dimensions <0.5 mm and was interpreted in the field to be either inorganic or charcoal. On the basis of its old age, relative to the majority of other samples from this site, we interpret this sample to be detrital.

We analyzed 16 samples from two trenches excavated into F1 and the capping loess wedge at the base of the F2/F1 riser face (Figure 8, main text). From trench T1NE-A, north of the fault, 2 samples were extracted from the colluvial material covering the riser face and 6 samples were collected from the underlying F1 terrace. Samples C-1 and C-5 were collected from within the colluvial gravels onlapping the F1 tread and range in age from 3.3-4.0 ka. Sample C-2 yielded an anomalously old age of ~22.3 ka. This sample exhibited a dull luster and was interpreted in the field to be either charcoal or inorganic. On the basis of its old age and its stratigraphic position relative to significantly younger samples, we interpret this sample to be detrital. From within the F1 terrace deposit, the only non-modern sample, C-4, yielded an age of 3.8 ± 0.1 ka. From trench T1SE-A, south of the fault and at the base of the southern F2/F1 riser segment, 7 samples were analyzed. Samples excavated from the overlying colluvial material from near the basal contact with the underlying F1 terrace included C-10, C-11, C-12, and C-13 (3.0-3.5 ka). Samples collected from within the F1 terrace included C-14, C-15, and C-16 (3.4-3.7 ka).

DR4. Radiocarbon (^{14}C) results from Yukuang

Here we discuss ^{14}C results from Yukuang (Table DR2). Results are presented beginning with the trenches excavated into T4 and T3, at the respective crest and base of the T4/T3 risers. We then discuss samples from trenches excavated into T3 and T2 at the crest and base of the T3/T2$_{east}$ riser, respectively. We conclude with a discussion of samples from trenches excavated into T2 and T1 at the crest and base of the T2/T1$_{east}$ riser, respectively.

We analyzed 7 samples from three trenches excavated into the T4 terrace deposit at the crest of the T4/T3 riser segments. Only samples C-83 and C-84 (0.73-2.72 ka) yielded Holocene ages and these samples were extracted from the silt capping the T4 tread. They exhibited woody root-like textures and were sampled in proximity to an extensive root network exposed in the trench wall, which leads us to classify these samples as roots. The remaining 5 samples exhibited dull luster and dark-gray color and yielded ages ranging from 24.2-58.4 ka. Samples C-79, C-82, and C-85 were collected from within the old alluvium and samples C-80 and C-81 were collected from within the T4 strath terrace and overlying silt, respectively. Sample C-80 yielded the youngest pre-Holocene age, but no minimum bound on the age could be calculated via currently available calibration techniques. Importantly, we think it is likely that this sample was reworked from the top of the underlying old alluvium. Thus, we take 24.2 ka as a maximum bound on the age of the sample.

We analyzed 5 samples from two trenches excavated into the T3 terrace and overlying silt material at the toe of the T4/T3 riser segments. From trench T3NE-A, samples C-66 (2.1 ± 0.1 ka) and C-67 (9.5 ± 0.2 ka) were collected from the silt material covering the riser face. From trench T3SE-A, sample C-71 (4.5 ± 0.6 ka) was collected from the silts capping the riser face. Samples C-72 and C-73 (36.7- >43.8 ka) were extracted from the colluvial gravel and the old alluvium, respectively, and they exhibited a dull luster and dark gray-color. We analyzed 8 samples from three trenches excavated into the T3 terrace at the crest of the $T3/T2_{east}$ riser segments. From trench T3NE-B, sample C-68 (6.4 ± 0.1 ka) was collected from the silt soil covering the T3 surface and the deeper samples, C-69 and C-70 (30.2-41.3 ka), were collected from within the old alluvium. Sample C-74 (32.9 ± 1.1 ka) was collected from the T3 strath terrace gravels in the downstream trench T3NE-B. Four samples from trench T3SW-A were collected from the T3 strath terrace deposit and underlying old alluvium. Samples C-75, C-76, and C-78 (1.18-2.12 ka) exhibited woody root-like morphologies and were collected in the context of an extensive root network. We interpret these samples to have been roots that grew into the T3 terrace following stream abandonment. Sample C-77 (27.0 ± 4.5 ka) was extracted from within the old alluvium and had a dull luster and gray color.

We analyzed 2 samples, C-60 (6.3 ± 0.1 ka) and C-61(5.4 ± 0.1 ka) from trench T2SE-A, which were collected from the silt material capping the base of the downstream $T3/T2_{east}$ riser segment. The samples were amber brown in color and exhibited morphologies of decayed woody plant fragments. We analyzed 8 samples from two trenches excavated into the T2 terrace at the crest of the $T2/T1_{east}$ riser segments. From the upstream trench T2NE-A, samples C-56 (4.2 ± 0.1 ka) and C-57 (4.1 ± 0.1 ka) were collected from within the T2 strath gravel conglomerate. Samples C-58 (5.8 ± 0.2 ka) and C-59 (33.3 ± 1.6 ka) were collected from within the old alluvium. From the downstream trench, T2SE-B, sample C-62 (5.1 ± 0.2 ka) was extracted from within the T2 strath gravel deposit and samples C-63, C-64, and C-65 (29.0-41.3 ka) were collected from the old alluvium. We analyzed 3 samples from trench T1NE-A, excavated into the silt material capping the toe of the downstream $T2/T1_{east}$ riser segment. These samples, C-53, C-54, and C-55 (3.8-4.0 ka) exhibited woody, plant fragment morphologies.

DR5. Keke Qiapu site

DR5.1 Results from the Keke Qiapu site

Keke Qiapu site description

The Keke Qiapu site is located 28 km east-northeast of Yukuang along the Qing Shui Quan reach of the ATF (Figure DR5 and Figure 10, main text). At this locality, three sub-parallel strands of the ATF intersect with the north-flowing ephemeral Keke Qiapu stream channel (Figure DR5). The most recent rupture is interpreted to have been concentrated on the northernmost fault strand because the mole track is well-developed and includes linear escarpments up to 4 m high, tectonic furrows with axes that trend 050-070°, and pressure ridges with axes that trend 020-070° (Figures DR5 and DR6). The tectonic furrows are characterized by closed depressions with ponded sediments within the mole track. The largest of these closed depressions is centered on the west stream bank, south of the T2 surface (Figure DR6). These recent tectonic features are superimposed on a 060-070° trending zone of disturbed topography that makes up the northernmost ATF mole track. Locally, the mole track has a fault-perpendicular width up to 55 m and reaches a maximum height of 4 m above the surrounding bajada surface. Approximately 3 km east-northeast along fault strike from the Keke Qiapu site, evidence for recent deformation distributed onto two sub-parallel fault strands was noted in the field. These strands were observed to cut latest Quaternary fan surfaces, some of which appear broadly correlative with those surfaces dated at Keke Qiapu. Though the central and southern ATF strands were not observed in the field at the location of the Keke Qiapu drainage, these strands have been previously mapped (Muretta, 2009). Furthermore, our own mapping via remotely sensed Corona imagery allowed us to extrapolate the fault traces along strike based on the observation of ~070° trending lineaments, upslope-facing escarpments, pressure ridges, and left-deflected stream channels (Figure DR5).

The Keke Qiapu site is located at the intersection of the north-flowing Keke Qiapu channel and the northernmost trace of the ATF (Figures DR5-DR7). At this position, the Keke Qiapu channel (T0) is incised 4.1-6.4 m vertically into T3 (Figure DR6). T3 is the most extensive surface and it exhibits a convex-up, alluvial fan morphology on the north side of the fault. T3 is blanketed with up to 25 cm of silt. Despite the cover of loess, channel and bar topography is well-preserved on the T3 surface, especially on the surfaces west of the modern stream channel. The bars are defined by boulders that crop out from the loess. Importantly, the T3 surfaces north and south of the fault and east and west of the stream bank have similar surface textures. The T2 and T1 surfaces are preserved on the flanks of the stream valley and are most extensive in the northwest and southeast quadrants of the map area, defined by the intersection of the stream channel and the ATF. The T2 and T1 surfaces north of the fault on the west stream bank are characterized by aligned gullies that trend ~305-340° and are spaced ~7-15 m apart. We speculate that these channels may have once aligned with the modern channel and the spacing may correlate to displacements associated with individual earthquake ruptures.

An additional feature of interest at Keke Qiapu is a trough on the T3 surface, which may represent a former stream channel (paleochannel) at the time when the stream occupied the T3 surface. South of the fault, the paleochannel is defined by 3 gullies that converge in a linear, north-northeast trending furrow (Figure DR6). This hollow is preserved both up- and downstream of the fault to the west of the modern stream. A cross-sectional exposure of the paleochannel on a north facing wall of the ATF mole track reveals a concave deposit of loess inset into the T3 surface that is in the same position as the topographic depression of the paleochannel (Figure DR7c). We interpret the loess to have accumulated following T3 abandonment.

We excavated two ~1.3 m-deep trenches into T3, one on either side of the fault (Figure DR6). Common stratigraphic units were observed in both trenches (Figure DR8a). The lowest package lies more than 60-70 cm below the modern surface and consists of horizontally stratified, well-indurated, angular gravel with coarse-sand matrix. We interpret this package to be an older alluvial deposit emplaced prior to T3 abandonment. The upper package lies more than 35-55 cm below the modern surface and consists of poorly consolidated gravels and boulders in a sand matrix. It differs from the underlying unit on the basis of its coarser grain size and weaker induration. We interpret this conglomerate to represent the final stream-occupation-related deposit. The surficial unit is a 5-25 cm thick package of stratified silts. We interpret the capping silt soil to have accumulated following abandonment of the T3 surface.

Keke Qiapu site offset data

The escarpment separating the T3 bajada from the inset T2 and T1 surfaces on the western bank of the stream shows an apparent left-lateral offset (Figure DR6). We define this feature as the T3/(T2-T1) riser. Projections of the riser crests into the fault zone yield a left-lateral offset of 33 ± 6 m. In addition to the faulted riser, a paleochannel on the T3 surface shows an apparent left-lateral offset (Figure DR6). Reconstruction of the paleochannel margins yields a similar left lateral offset as the T3/(T2-T1) riser of 33 ± 8 m. The similarity in offset between the paleochannel and faulted riser suggests that the T3 surface abandonment age should closely approximates the age of both of these faulted features (e.g., Cowgill, 2007). But the up- and downstream paleochannel margins may (1) not-correlate, in which case the similarity in offset between the paleochannel and the T3/(T2-T1 riser) is not meaningful or (2) have formed by gullying after abandonment of the T3 surface, in which case the offset does not correspond to abandonment of the T3 surface. Below we explore scenarios that explore a variety of reconstructions.

Keke Qiapu site age data

No organic materials suitable for ^{14}C dating were identified at Keke Qiapu. Instead, we dated pedogenic carbonate rinds coating terrace gravels extracted from the SW Pit using the $^{230}Th/U$ method (Table DR3, Figures DR9 and DR10) and amalgamated quartz-rich clasts from the same trench using the TCN ^{10}Be method (Table DR4, Figure DR8). We obtained $^{230}Th/U$ analyses from 6 sub-samples from 2 clasts, extracted 50 cm from below the T3 surface from within the upper T3 deposit. Ages were corrected for initial ^{230}Th using the approach of Ludwig and Paces (2002). That is, ^{232}Th was used as an index of detrital contamination, detritus was assumed to have a typical upper crustal U/Th ratio and $^{230}Th/^{238}U$ and $^{234}U/^{238}U$ ratios in secular equilibrium, and generous uncertainties in the assumed ratios were propagated into final ages; i.e., $^{232}Th/^{238}U = 1.2 \pm 0.5$, $^{230}Th/^{238}U = 1.0 \pm 0.25$, and $^{234}U/^{238}U = 1.0 \pm 0.25$. Ages for sub-samples from each clast are in satisfactory agreement, consistent with closed U/Th systems and the absence of inherited coatings. The weighted mean age of the three sub-samples from clast B12 (17.1 ± 2.1 ka) is interpreted as a minimum depositional age for the upper T3 alluvium.

To further constrain the age of the T3 surface, we processed a depth profile of amalgamated quartz-rich clasts from the same trench using the TCN ^{10}Be method. As Table DR4 and Figure DR8 indicate, ^{10}Be concentrations generally decrease with increasing depth, with the exception of the sample collected from 50 cm below the surface. We calculated three model ages to constrain the timing of T3 abandonment and to test whether the upper and lower T3 terrace deposits are members of the same depositional sequence. The first calculation is based on a regression through all of the data points and yields an exposure age of 6.6 ± 2.1 ka (Figure DR8b). The second regression excludes the 50 cm datum and yields a model age of 7.6 ± 0.8 ka (Figure DR8c). Both of these age calculations assume that the upper and lower T3 terrace deposits are part of the same sequence, with little time separating their deposition. We also made a model age calculation by treating the upper sample population separately. This regression, based on the 25 and 50 cm data points, yields an age of 10.8 ± 1.8 ka, assuming uniform inherited ^{10}Be in the upper T3 gravel, and no erosion or inflation of the T3 surface after alluvial deposition (Figure DR8d). Importantly, this age is consistent with a model in which the upper T3 deposit postdates the lower T3 deposit.

DR5.2. Discussion of Keke Qiapu site

Keke Qiapu site terrace ages

The U-series and ^{10}Be depth profile dating applied to clasts from the SW Pit at the Keke Qiapu site provides age control for abandonment of the T3 surface on the south side of the northernmost strand of the ATF (Figure DR8 and DR10). These two independent geochronologic techniques yielded, respectively, results of 17.1 ± 2.1 ka and 10.6 ± 1.8 ka for the uppermost terrace alluvium (samples from 25 and 50 cm below the surface). These age determinations are significantly older than the model ages determined from consideration of the entire TCN depth profile, which integrated measurements from the upper and lower T3 deposits. In light of the stratigraphic differences between the upper and lower T3 deposits as well as these geochronologic results, we interpret the upper T3 deposit to significantly post-date the older/lower T3 deposit. This interpretation accounts for the shift in ^{10}Be concentrations across this stratigraphic boundary and indicates that the regression calculations that include samples from the lower T3 deposit overestimate inherited ^{10}Be, leading to an age for the upper T3 alluvium that is too young. No age control was determined for the T3 surface north of the ATF.

We propose that the $^{230}Th/U$ age of 17.1 ± 2.1 ka provides a reliable minimum age for the emplacement of the T3 surface south of the ATF. This is our preferred age because the ^{10}Be model age regression is only constrained by two samples (Figure DR8d). Furthermore, we note that the T3 age determined at Keke Qiapu is approximately synchronous with periods of terrace formation determined at other sites in northern Tibet, including 16.6 ± 3.9 ka at the Cherchen He site (Mériaux et al., 2004), 16.4 ± 1.9 ka in central Tibet (Blisniuk and Sharp, 2003), and 15.1 ± 0.7 ka (Harkins and Kirby, 2008) along the central and eastern Kunlun Fault, respectively, as expected if fan-surface formation is in part controlled by regional climatic processes and occurs in a pulsed and synchronized manner (e.g., Peltzer et al., 1989; Bull, 1990, 1991).

No ages were determined for the inset T2 and T1 surfaces at Keke Qiapu. To aid in bracketing the riser age at this site, we consider the youngest terrace age from the nearby Yuemake site (Cowgill et al., 2009), ~33 km to the north east along the Qing Shui Quan reach of the ATF (Figure 10, main text). This terrace age extrapolation method follows the protocol of previous morphochronologic investigations in the Indo-Asian region (Mériaux et al., 2004; e.g., Li et al., 2005; Mériaux et al., 2005), in which local age data are unavailable to directly date faulted landforms. At Yuemake, the T2 surface was bracketed to have formed between 2.35-2.06 ka by ^{14}C ages determined from organic material collected from within the terrace deposit and overlying silt deposits. This terrace surface represents the youngest terrace age determined along this reach of fault. Furthermore, it displays similar surface characteristics and height (~3 m) above the modern drainage when compared to T2 at Keke Qiapu (2 m above the modern drainage). The age extrapolation proposed here is speculative and is only valid under the assumption that terrace forming events are driven by regional climatic modulation (e.g., Bull, 1990, 1991) and that the T2 surfaces at these sites are correlative.

Keke Qiapu site bounds on slip rate

At Keke Qiapu, the faulted T3/(T2+T1) riser is left-laterally offset 33 ± 6 m, which is broadly similar to the observed offset (33 ± 8 m) of the loess-filled paleochannel on the T3 surface. If the reconstruction of the paleochannel margins is robust, then the similarity in offset between this feature and the T3/(T2+T1) riser indicates that upper T3 surface abandonment age most closely approximates the age of both of these faulted features (e.g., Cowgill, 2007). In this reconstruction scenario, the T3 surface was occupied by the stream channel, which carved the paleochannel. Shortly after forming the paleochannel, the stream avulsed to the east and then incised to form the T3/T2+T1 riser. A slip rate of 1.9 ± 0.4 mm/yr is calculated by pairing the 33 ± 6 m displacement with the T3 surface age of 17.1 ± 2.1 ka (Table 1, main text). This rate is significantly lower than the range of rates determined at the other sites explored in this study (Kelutelage and Yukuang) and at the adjacent Yuemake site (Cowgill et al., 2009). This result may indicate that correlation of the paleochannel segments at the site is erroneous or that this feature formed after the T3 surface was incised. An alternative slip rate can be calculated by using the age of the T2 surface from Yuemake (2.35-2.06 ka) as a proxy for the inset T2 age at Keke Qiapu, which yields a maximum slip rate of 15.0 ± 2.8 mm/yr. Importantly, this result does not follow the type-3 control for potential cross-fault terrace riser diachroneity. Furthermore, this reconstruction does not account for displacement that may have occurred on the central and southern ATF strands. Four hypotheses are proposed below to explore a range of plausible site evolution scenarios for this site (Figure DR11). In the latter three scenarios, we treat the paleochannel as a secondary feature that formed after incision of T3.

In the first scenario, deformation has been distributed on the three parallel fault strands of the ATF at this site (Figure DR11, scenario 1). Because the faulted T3/(T2+T1) riser is only displaced by the northernmost fault strand, this riser does not record additional displacement that may have occurred on the more southerly fault strands. Thus, some percentage of deformation may be missing by only considering the northern fault strand. This scenario could be consistent with reconstruction of the paleochannel and T3/(T2+T1) riser in combination with the T3 surface abandonment age. This is not a preferred scenario, because the surface expression of the more southerly fault strands is significantly more subdued than that observed along the northern fault strand, which leads us to conclude that it is most likely that the majority of late Quaternary deformation at Keke Qiapu has been focused on the northern fault strand.

In the second scenario, the stream channel deposited the T3 surfaces at ~17.1 ka and then stream flow ceased for a period of ~12-13 kyr (Figure DR11, scenario 2). During this interval, the once connected T3 surfaces were left-laterally transported away from each other. Stream flow resumed at ~2-3 ka, leading to incision and formation of the T3/(T2+T1) riser. The riser was subsequently left-laterally displaced ~33 m. We do not think this is a likely scenario, given regional climatic records which suggest that mid Holocene was characterized by general warming and precipitation (e.g., Gasse et al., 1991), inconsistent with a dearth of stream activity. Furthermore, this type of behavior has not been observed at sites along strike.

A third scenario is one in which an isochronous regional bajada surface (T3) was deposited on the north side of the fault at ~17.1 ka (Figure DR11, scenario 3). In this scenario, the bajada was left laterally faulted and the feeder stream channels were left deflected and/or beheaded. Prior to ~2.2 ka, a feeder channel to the east of the modern Keke Qiapu drainage was beheaded and then the northern half of the stream channel aligned with and captured the southern

Keke Qiapu channel. At this time, the reconfigured stream channel incised the T3 surface and created the T3/(T2+T1) riser. Subsequently, the riser was left-laterally offset ~33 m. A candidate feeder channel is located ~115 m east of the modern channel. Retro-deforming the landscape ~150 m from the modern configuration aligns the T3/(T2+T1) riser with the feeder channel and also results in the alignment of several other mapped channels (displacement is approximate because it was determined from a Corona scene that is neither georeferenced nor rectified). Admittedly this solution is non-unique. This reconstruction yields an approximate slip rate of ~8.8 mm/yr by pairing the T3 abandonment age with a displacement of 150 m. This model predicts isochronous T3 ages north and south of the fault, which is consistent with the observation of similar surface characteristics, north and south of the fault, as well as matching stratigraphic packages from the SW and NW pits. This scenario does not rule out the possibility of some component of deformation occurring on the more southern ATF strands.

A fourth scenario that can reconcile these observations is one in which the southern and northern fan deposits do not match (Figure DR11, scenario 4). In this scenario, the upstream T3 surface was deposited at ~17.1 ka and then the stream channel incised <1 m into the upstream T3 surface. Following this incision, the stream channel was confined to the width of the observed modern stream channel. During subsequent faulting, the confined upstream channel deposited material on the north side of the fault across and onto the regional bajada with minimal incision. During this interval, material was left-laterally transported away from the stream channel and new (younger) fans were deposited north of the ATF. Importantly, prior to ~2.2 ka, the stream channel deposited an alluvial fan, which was then incised to create the T3/(T2+T1) riser. This riser was then left-laterally offset ~33 m. This scenario predicts diachronous T3 surface ages on opposite sides of the fault. In particular, a younger T3 surface age is predicted north of the fault at the crest of the northern T3/(T2+T1) riser segment. This prediction is inconsistent with our observation of correlative, cross-fault T3 surfaces and stratigraphic sequences and this is not our preferred model.

In summary, scenario 3 best matches the current observations and data, the strongest of which include the presence of a candidate feeder channel east of the modern channel and the similarity of the cross-fault T3 surfaces and stratigraphic sequences. Additional age control from the northern T3 surface at the crest of the T3/(T2+T1) riser segment and the inset T2 surface will further strengthen the reconstruction and slip-rate derivation for this site. Given that additional data are needed to firmly distinguish between the various scenarios, we submit the most conservative slip rate from the faulted T3/(T2+T1) riser at Keke Qiapu ranges 1.9-15.0 mm/yr, calculated by pairing the T3 and inferred T2 ages with the observed offset.

DR6. U-series samples and methods

Carbonate rinds that coat the bottom of fluvial gravels associated with terrace deposits at Keke Qiapu were dated using the ^{230}Th/U system to provide a minimum age of these deposits (e.g., Blisniuk and Sharp, 2003; Sharp et al., 2003). Application of the U-series system to date the age of pedogenic carbonates focuses on the relationship between ^{230}Th (half-life 75.69 ka) and its immediate parent ^{234}U (half-life 245.25 ka), which in turn is produced by decay of the parent isotope ^{238}U (half-life 4.47 Ga). In a closed system, this decay chain will reach a state of secular equilibrium, in which the number of decay events per unit time (the activity) of each nuclide in the chain is equal. At the time of deposition, a carbonate rind will not be in secular equilibrium and instead will be depleted in ^{230}Th and enriched in ^{234}U relative to equilibrium because uranium is significantly more soluble than thorium in the soil waters from which carbonate rinds are precipitated. Measurement of the isotopic ratios ^{230}Th/^{238}U and ^{234}U/^{238}U can resolve production of ^{230}Th and decay of ^{234}U toward secular equilibrium. Importantly, initial ^{230}Th within a carbonate rind must be subtracted in order to obtain accurate ages, which we addressed by applying a correction indexed to the measured ^{232}Th contents of the samples (e.g., Ludwig, 2008).

We sampled carbonate rinds from two clasts excavated from 50 cm below the surface in Pit SW at Keke Qiapu (Table DR3). The clasts were cut, polished, and cleaned ultrasonically. We reviewed and photographed the samples under 6-50 *X* magnification to identify internal stratigraphy. The carbonate material was amber-colored in cross-section and dark brown in plan view. The carbonate was dense and free of visible detritus. Total rind thicknesses ranged from 0.2-0.5 mm and within rinds, sub-0.1 mm thick lamina were identified (Figure DR9). We removed six, ~8-12 mg aliquots of carbonate using a "moat-and-spall" technique that resulted in a combination of small fragments and powdered sample. The rinds were sufficiently thin and dense to prevent extraction of microstratigraphic layers. This bulk sample approach has the disadvantage that the entire age interval over which the carbonate rinds formatted is averaged within the analyzed aliquot of carbonate material. The samples underwent total dissolution in concentrated HNO_3 and HF and were spiked with ^{233}U-^{236}U-^{229}Th. Following U and Th extraction via column ion exchange methods, the samples were loaded as colloidal graphite sandwiches onto rhenium filaments and then isotopically analyzed via Micromass Sector-54 TIMS. Ages and uncertainties were determined using Isoplot 3.7 (Ludwig, 2008). All uncertainties are given at the 95% confidence interval.

DR7. ^{10}Be samples

To constrain the age of tread abandonment at Keke Qiapu, we measured concentrations of the in-situ TCN ^{10}Be (e.g., Lal, 1991; Gosse and Phillips, 2001) in amalgamated samples of quartz-rich gravel collected from a depth profile excavated into a terrace deposit. We followed the sub-surface sampling technique (Anderson et al., 1996; Repka et al., 1997; Hancock et al., 1999) to discriminate the inherited TCN component from the post-depositional TCN component. This latter component is the value used to determine the exposure age of a fluvial deposit. We followed the sample preparation, processing, and analysis procedures as well as the exposure-age calculation method described by Gold et al. (2009).

At Keke Qiapu, five aggregated gravel samples were collected from the SW Pit, which lies upstream of the mole track (Table DR4). Samples were collected at depths of 25, 50, 75, 100, and 125 cm. We measured sample depths from the modern surface to the center of the sampled zone, each of which was 6 cm thick. Each aggregate interval consisted of ≥53 clasts of quartz-rich granitoid or gneiss, 2-15 cm in diameter. The 25 and 50 cm zones were sampled from within the intermediate gravel conglomerate, which we interpret to be the upper T3 terrace deposit (Figure DR8). In contrast, the 75, 100, and 125 cm zones were collected from the lower consolidated gravel deposit, which we interpret to be a lower and older package of the T3 deposit (Figure DR8). We anticipated that the ^{10}Be concentration results might be scattered due to our sampling across a stratigraphic intervals. Evaluating the time interval between depositional of the stratigraphic layers was an additional goal of this sampling strategy.

References cited in supplemental files

Anderson, R. S., Repka, J. L., and Dick, G. S., 1996, Explicit treatment of inheritance in dating depositional surfaces using in situ 10Be and 26Al: Geology, v. 24, no. 1, p. 47-51.

Blisniuk, P. M., and Sharp, W. D., 2003, Rates of late Quaternary normal faulting in central Tibet from U-series dating of pedogenic carbonate in displaced fluvial gravel deposits: Earth and Planetary Science Letters, v. 215, no. 1, p. 169-186.

Bronk Ramsey, C., 1995, Radiocarbon calibration and analysis of stratigraphy: The OxCal program: Radiocarbon, v. 37, no. 2, p. 425-430.

-, 2001, Development of the radiocarbon calibration program OxCal: Radiocarbon, v. 43, no. 2A, p. 355-363.

Bull, W. B., 1990, Stream-terrace genesis: implications for soil development: Geomorphology, v. 3, p. 351-367.

-, 1991, Geomorphic Responses to Climatic Change: New York, Oxford University Press, 326 p.

Cowgill, E., 2007, Impact of riser reconstructions on estimation of secular variation in rates of strike–slip faulting: Revisiting the Cherchen River site along the Altyn Tagh Fault, NW China: Earth and Planetary Science Letters, v. 254, no. 3-4, p. 239-255.

Cowgill, E., Gold, R. D., Chen, X., Wang, X.-F., Arrowsmith, J. R., and Southon, J. R., 2009, Low Quaternary slip rate reconciles geodetic and geologic rates along the Altyn Tagh fault, northwestern Tibet: Geology, v. 37, no. 7, p. 647-650.

Dubrule, O., 1983, Two methods with different objectives: Splines and kriging: Mathematical Geology, v. 15, no. 2, p. 245-147.

Gasse, F., Arnold, M., Fontes, J. C., Fort, M., Gibert, E., Huc, A., Li, B., Li, Y., Liu, Q., Mélieres, F., Van Campo, E., Wang, F., and Zhang, Q., 1991, A 13,000-year climate record from western Tibet: Nature, v. 353, p. 742-745.

Gold, R. D., Cowgill, E., Arrowsmith, J. R., Gosse, J., Wang, X., and Chen, X., 2009, Riser diachroneity, lateral erosion, and uncertainty in rates of strike-slip faulting: A case study from Tuzidun along the Altyn Tagh Fault, NW China.: Journal of Geophysical Research, B, Solid Earth and Planets, v. 114, no. B04401.

Gosse, J. C., and Phillips, F. M., 2001, Terrestrial in situ cosmogenic nuclides: theory and application: Quaternary Science Reviews, v. 20, no. 14, p. 1475-1560.

Hancock, G. S., Anderson, R. S., Chadwick, O., and Finkel, R., 1999, Dating fluvial terraces with 10Be and 26Al profiles: application to the Wind River, Wyoming: Geomorphology, v. 27, p. 41-60.

Harkins, N., and Kirby, E., 2008, Fluvial terrace riser degradation and determination of slip rates on strike-slip faults: An example from the Kunlun fault, China: Geophysical Research Letters, v. 35, no. L05406, p. doi:10.1029/2007GL033073.

Lal, D., 1991, Cosmic ray labeling of erosion surfaces: *in situ* nuclide production rates and erosion: Earth and Planetary Science Letters, v. 104, p. 424-439.

Li, H., Van der Woerd, J., Tapponnier, P., Klinger, Y., Xuexiang, Q., Jingsui, Y., and Yintang, Z., 2005, Slip rate on the Kunlun fault at Hongshui Gou, and recurrence time of great events comparable to the 14/11/2001, Mw ~7.9 Kokoxili earthquake Earth and Planetary Science Letters, v. 237, no. 1-2, p. 285-299.

Ludwig, K. R., 2008, User's manual for Isoplot 3.70: A geochronologic toolkit for Microsoft Excel: Berkeley Geochronology Center Special Publication, v. 4, p. 1-77.

Mériaux, A., Tapponnier, P., Ryerson, F. J., Xiwei, X., King, G., Van der Woerd, J., Finkel, R., Haibing, L., Caffee, M., Zhiqin, X., and Wenbin, C., 2005, The Aksay segment of the northern Altyn Tagh fault: Tectonic geomorphology, landscape evolution, and Holocene slip rate: Journal of Geophysical Research, v. 110, no. B4, p. 1-32.

Mériaux, A.-S., Ryerson, F. J., Tapponnier, P., Van der Woerd, J., Finkel, R., Xiwei, X., Xiwei, X., and Caffee, M., 2004, Rapid slip along the central Altyn Tagh Fault: Morphochronologic evidence from Cherchen He and Sulamu Tagh: Journal of Geophysical Research, v. 109, no. B6.

Muretta, M., 2009, Holocene earthquake geology of the central Altyn Tagh Fault, Xinjiang China: Implications for recurrence interval, strain release rate, and fault behavior: Arizona State University, 146 p.

Peltzer, G., Tapponnier, P., and Armijo, R., 1989, Magnitude of late Quaternary left-lateral displacements along the north edge of Tibet: Science, v. 246, no. 4935, p. 1285-1289.

Reimer, P. J., Baillie, M. G. L., Bard, E., Bayliss, A., Beck, J. W., Bertrand, C. J. H., Blackwell, P. G., Buck, C. E., Burr, G. S., Cutler, K. B., Damon, P. E., Edwards, R. L., Fairbanks, R. G., Friedrich, M., Guilderson, T. P., Hogg, A. G., Hughen, K. A., Kromer, B., McCormac, G., Manning, S., Ramsey, C. B., Reimer, R. W., Remmele, S., Southon, J. R., Stuiver, M., Talamo, S., Taylor, F. W., van der Plicht, J., and Weyhenmeyer, C. E., 2004, IntCal04 terrestrial radiocarbon age calibration, 0-26 cal kyr BP: Radiocarbon, v. 46, no. 3, p. 1029-1058.

Repka, J. L., Anderson, R. S., and Finkel, R. C., 1997, Cosmogenic dating of fluvial terraces, Fremont River, Utah: Earth and Planetary Science Letters, v. 152, p. 59-73.

Sharp, W. D., Ludwig, K. R., Chadwick, O. A., Amundson, R., and Glaser, L. L., 2003, Dating fluvial terraces by 230Th/U on pedogenic carbonate, Wind River Basin, Wyoming: Quaternary Research, v. 59, no. 2, p. 139-150.

Supplemental Materials Tables

Table DR1. ^{14}C AMS analyses from Kelutelage

Table DR2. ^{14}C AMS analyses from Yukuang

Table DR3. ^{230}Th/U geochronology at Keke Qiapu

Table DR4. Keke Qiapu ^{10}Be geochronology

Supplemental Materials Figures

Figure DR1.

Quickbird image of the Kelutelage site. Arrows on the margins of the image indicate the location of the principle trace of the ATF. The orthorectified image has a ground resolution of 0.60 m, was acquired on December 27th, 2006, and was obtained from Digital Globe.

Figure DR2.

Topographic and neotectonic map of Kelutelage. (a) Uninterpreted hillshaded digital terrain model (DTM) derived from a T-LiDAR survey (cell size 0.3 m). (b) Neotectonic observations and 0.5 m contour map overlain on DTM (same as in Figure 5, main text).

Figure DR3.

Quickbird image of Yukuang. Arrows on the margins of the image indicate the location of the principle trace of the ATF. The active channel is white due to the band combination used to accentuate fault-related features. The orthorectified image has a ground resolution of 0.60 m, was acquired on February 14th, 2007, and was obtained from Digital Globe.

Figure DR4.

Topographic and neotectonic map of Yukuang. (a) Uninterpreted hillshaded DTM derived from a topographic survey conducted with a total station including breaklines and topographic points (cell size 0.5 m). (b) Neotectonic observations and 0.5 m contour map overlain on hillshaded DTM (same as Figure 11, main text).

Figure DR5.

Corona image of the Keke Qiapu site. (a) Uninterpreted and (b) mapped 12.5 km long swath of the central ATF centered on the Keke Qiapu site. Importantly, the ATF is multi-stranded in proximity to Keke Qiapu. Mapping conducted on the basis of reconnaissance observations made east of the Keke Qiapu site and extrapolated into the Keke Qiapu site using remotely sensed observations of drainage-perpendicular lineaments, upslope-facing escarpments, pressure ridges, and left-deflected stream channels. (c) Overview of the Keke Qiapu site, with fault traces and streams mapped. The Corona scene is neither georeferenced nor rectified, so the scale bar and orientation are approximate. The image was acquired on November 6, 1968 and was obtained from the United States Geological Survey Earth Resource Observation and Science Data Center. Scene identification number is DS1105-1039DF146.

Figure DR6.

Neotectonic and topographic map of the Keke Qiapu site. Topography derived from a topographic survey conducted with a total station. (a) Uninterpreted hillshaded DTM (cell size 0.5 m). (b) Neotectonic observations and 0.5 m contour map overlain on hillshaded DTM. Contacts were mapped in the field using a total station and stereo Corona images. The Keke Qiapu site is located at the intersection of a north-flowing channel and the sub-perpendicular-striking ATF. Above the modern channel (T0), three abandoned terrace surfaces are preserved (T1-T3). The left-laterally offset T3/(T2+T1) riser and paleochannel are indicated.

Figure DR7.

Photographs showing key field relationships at Keke Qiapu. (a) South-looking view of the northern and (b) north-looking view of southern portions of the field site, showing the left-laterally offset T3/(T2+T1) riser segments. (c) Upstream paleochannel, infilled with loess. Decorations and orientations match conventions in Figure 6. Photograph locations and view directions indicated in Figure DR6. People standing 1.7-1.9 m tall in photographs indicated with yellow ellipses, with the exception of panel (c) where scale is indicated by a map board (~0.5 m wide) at the crest of the silt-filled paleochannel.

Figure DR8.

T3 stratigraphy and ^{10}Be geochronology at Keke Qiapu. (a) Composite stratigraphic column and photograph depicting the stratigraphic relationships observed in the trenches excavated into the T3 surface at Keke Qiapu. Three distinct depositional layers are defined. Exponential regression through TCN depth profile from amalgamated gravels extracted from the SW Pit at Keke Qiapu calculated using (b) all of the data (c) all of the data except the 50 cm interval outlier, and (d) the upper two intervals. The exponential fit through the upper two samples, collected from the uppermost depositional layer (d), yields an age of 10.7 ± 1.8 ka (calculation made by fixing the inheritance of ^{10}Be at zero at 500 cm below the surface). The offset in ^{10}Be concentration between the upper and lower T3 deposits supports the interpretation that there was a significant time lag between deposition of the upper and lower T3 deposits. Model age calculations follow the methods described in Gold et al. (2009).

Figure DR9.

Photographs of carbonate rinds analyzed in U-Series analyses. (a) B5 clasts and (b) B5 cross-section, showing rind analyzed in aliquot B5sub3. (c) B12 clast and (d) B12 cross-section, showing rind analyzed in aliquot B12sub2.

Figure DR10.

$^{234}U/^{238}U$-$^{230}Th/^{238}U$ evolution diagram showing analyses of pedogenic carbonate pebble coats from soil of T3 surface at Keke Qiapu. Three sub-samples from clast B12 (stippled) and two from clast B5 (no fill) are shown; steeply inclined lines are isochrons labeled in ka; nearly horizontal lines are initial $^{234}U/^{238}U$ activity ratios. Weighted mean of B12 sub-samples, 17.1 ±

2.1 ka, is interpreted as a minimum age for upper T3 alluvium. Error ellipses are 2-σ. One imprecise analysis of clast B5 is omitted for clarity.

Figure DR11.

Four possible reconstructions for the Keke Qiapu site. In the first, slip is distributed across three fault strands (fault traces match mapping presented in Figure 14, main text). In the second, the Keke Qiapu stream shuts-off in the interval from ~17.1 to >~2.2 ka (fault trace and stream positions are schematic). In scenario 3, a beheaded feeder channel captures the Keke Qiapu channel prior to ~2.2 ka (fault trace and channel positions mapped from the underlying Corona image). In scenario 4, the northern bajada surface is younger from west to east, relative to the Keke Qiapu channel and the offset of the T3/(T2+T1) riser corresponds to incision of the most recent >~2.2 ka fan (fault trace and stream positions are schematic). Scenario 3 is considered the most likely because the T3 surfaces, north and south of the fault, display similar surface characteristics and the cross-fault trenches revealed matching stratigraphic packages.

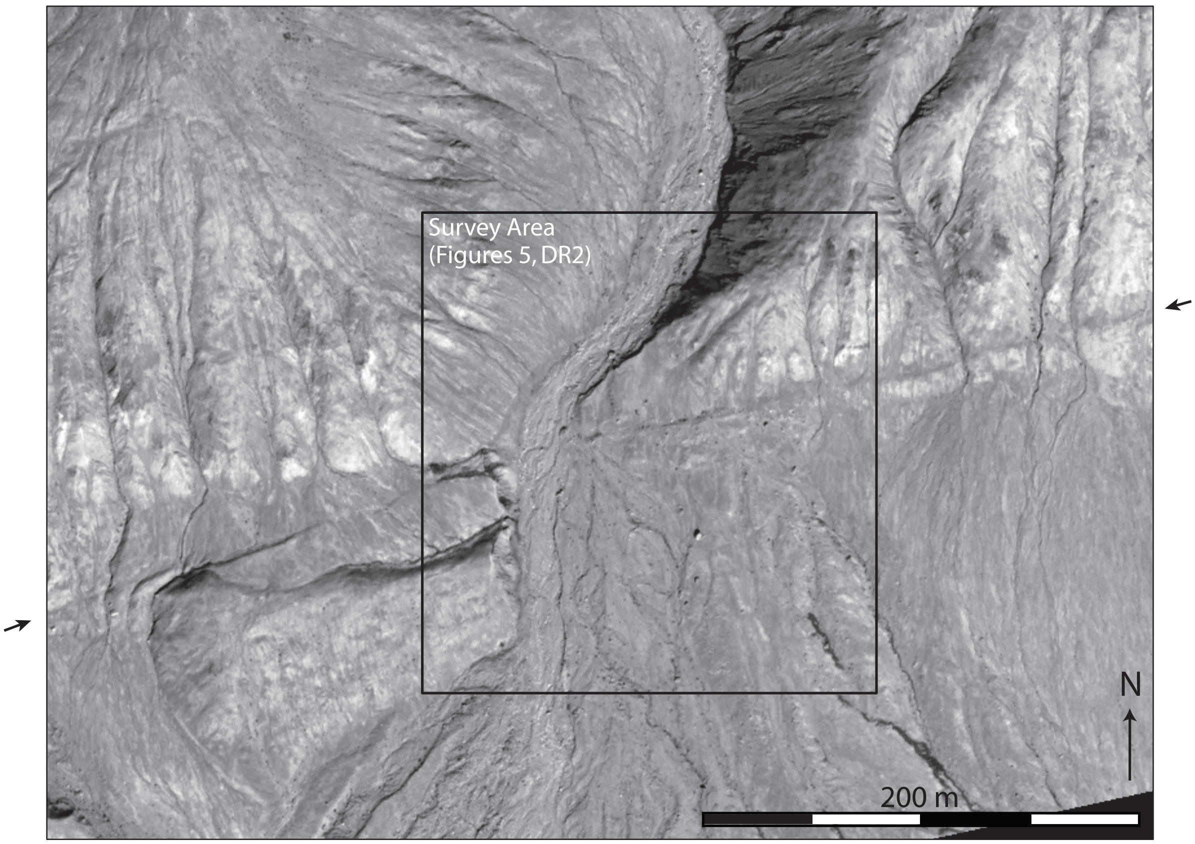

Figure DR1. Kelutelage overview.

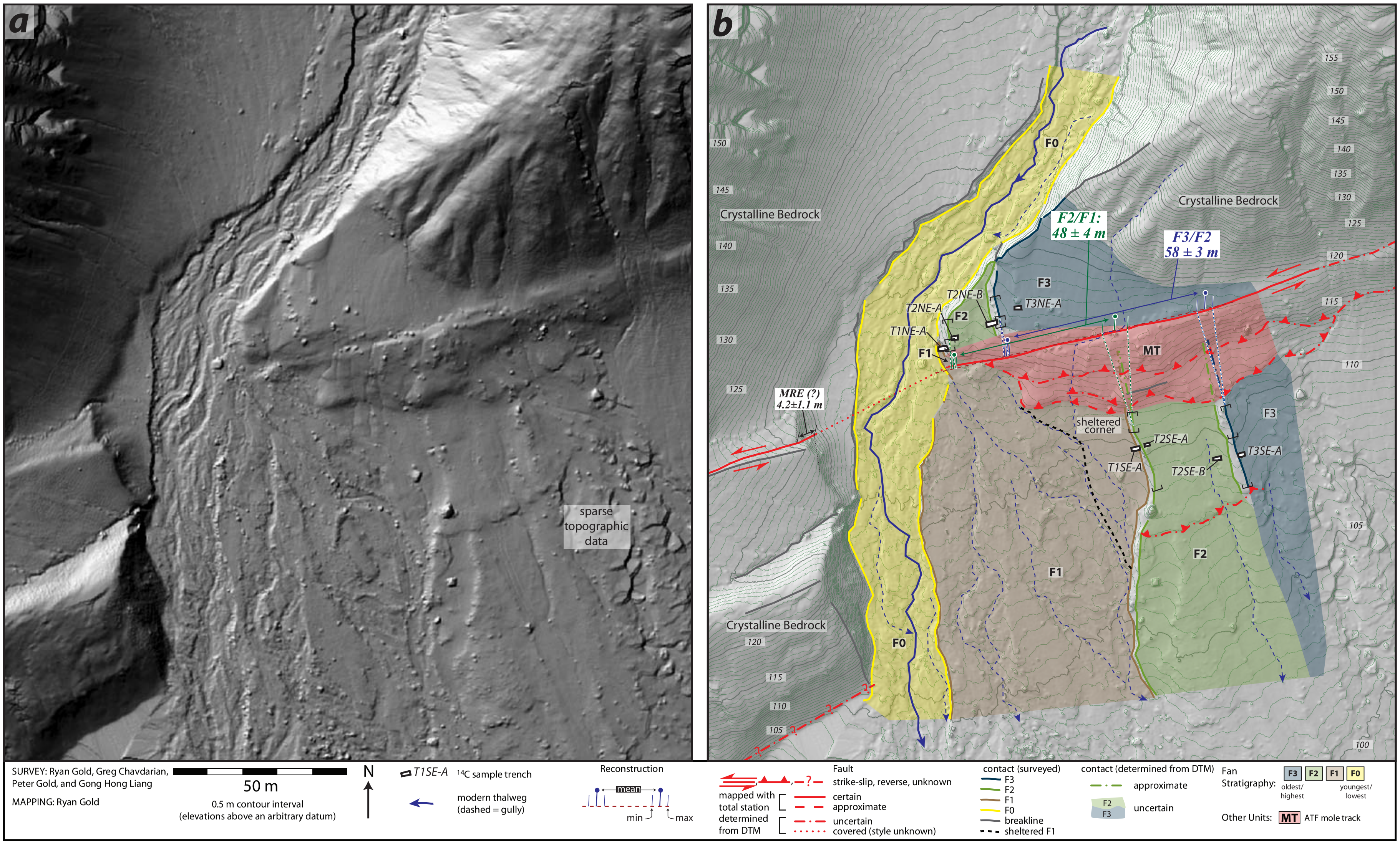

Figure DR2. Topographic and neotectonic map of Kelutelage.

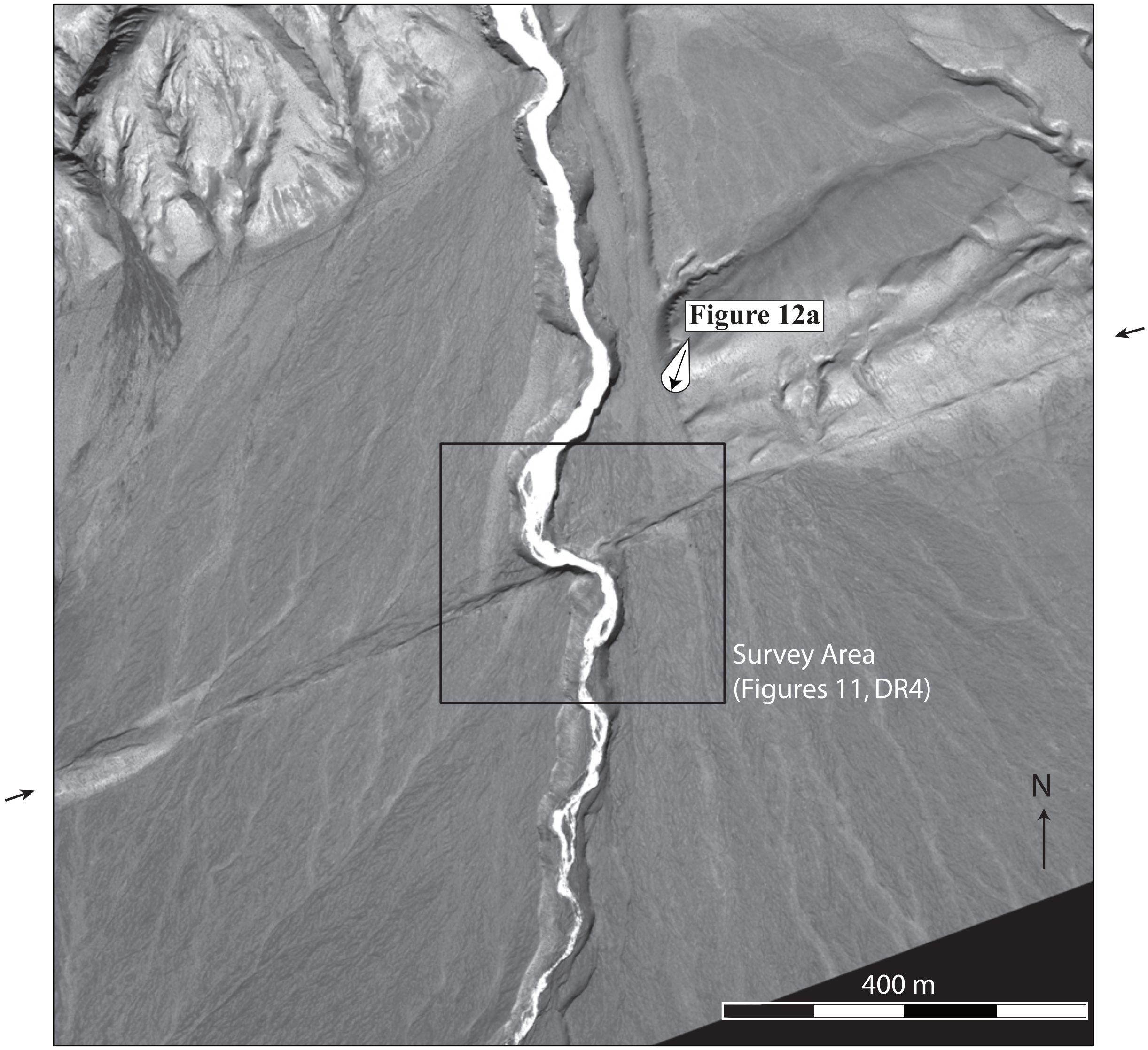

Figure DR3. Yukuang overview.

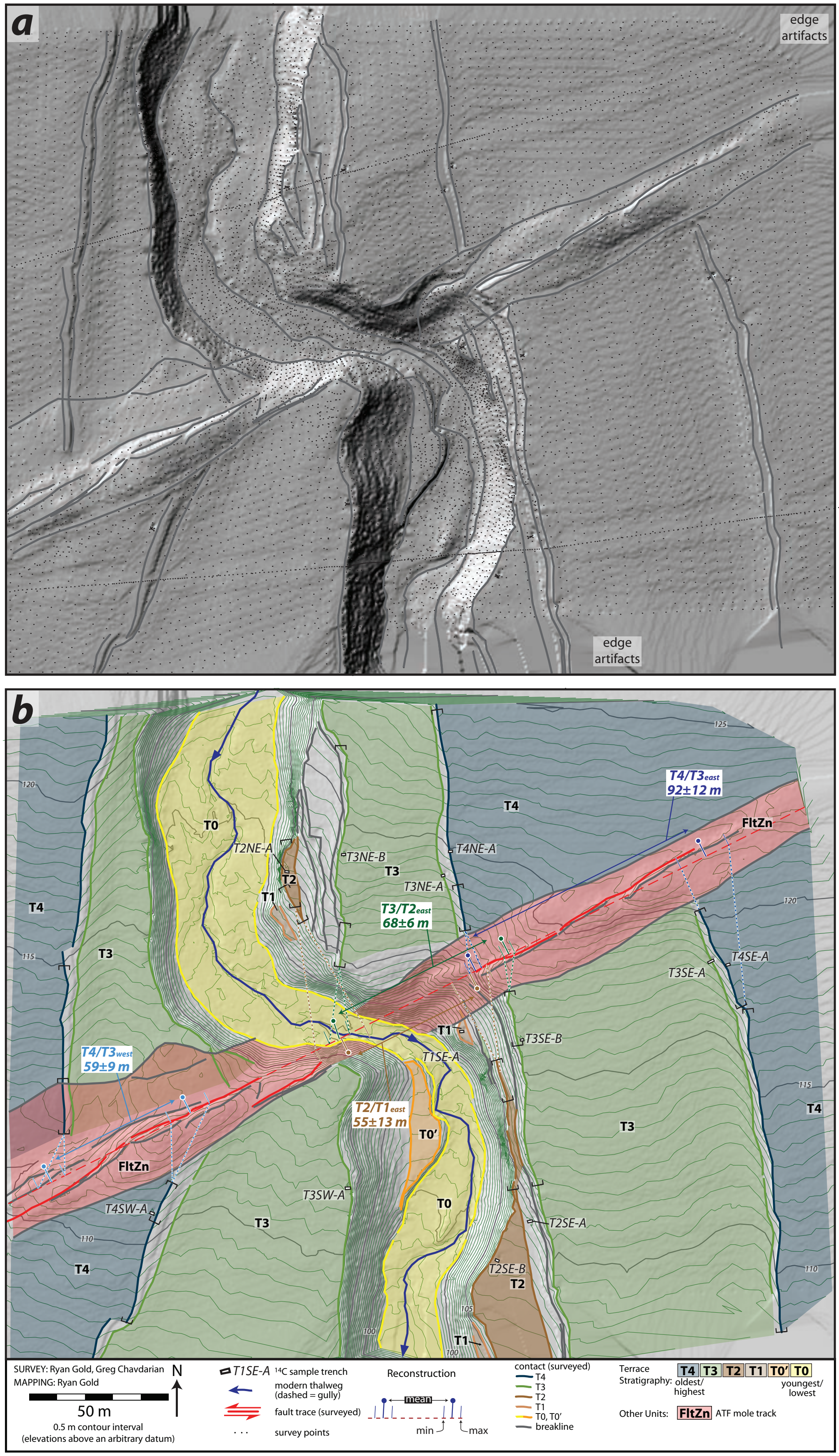

Figure DR4. Topographic and neotectonic map of Yukuang.

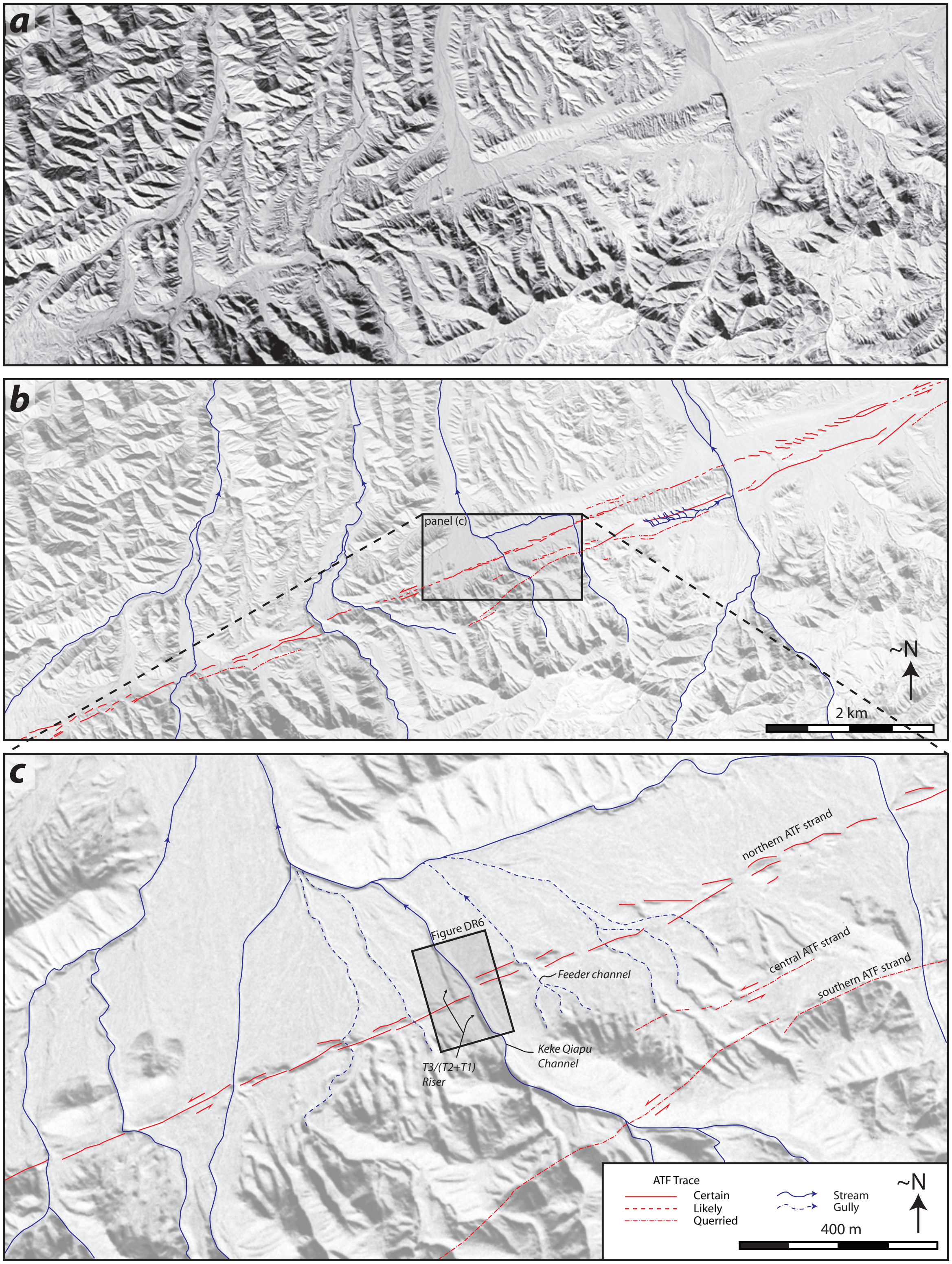

Figure DR5. Corona image of the Keke Qiapu site.

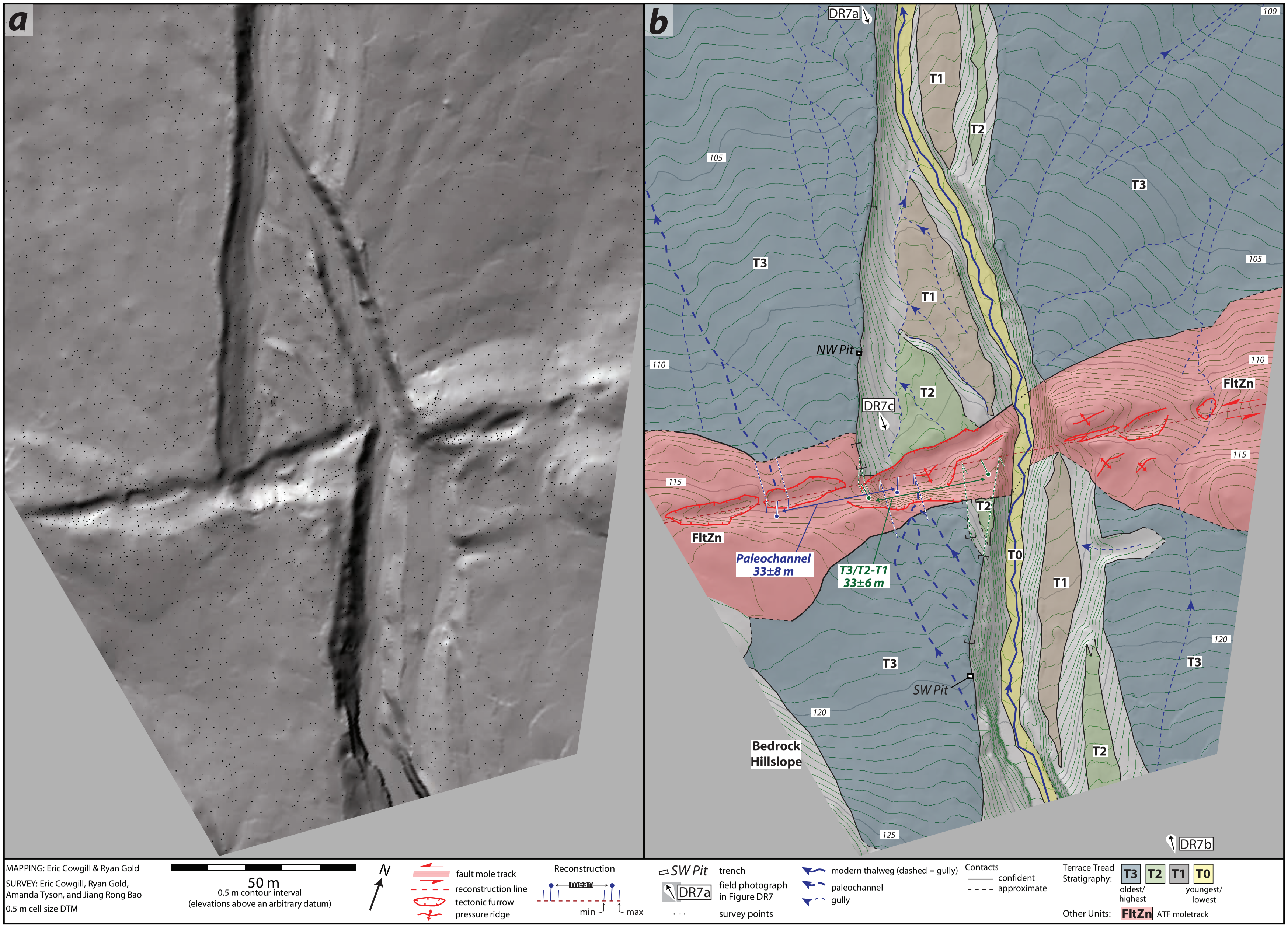

Figure DR6. Neotectonic and topographic map of the Keke Qiapu site.

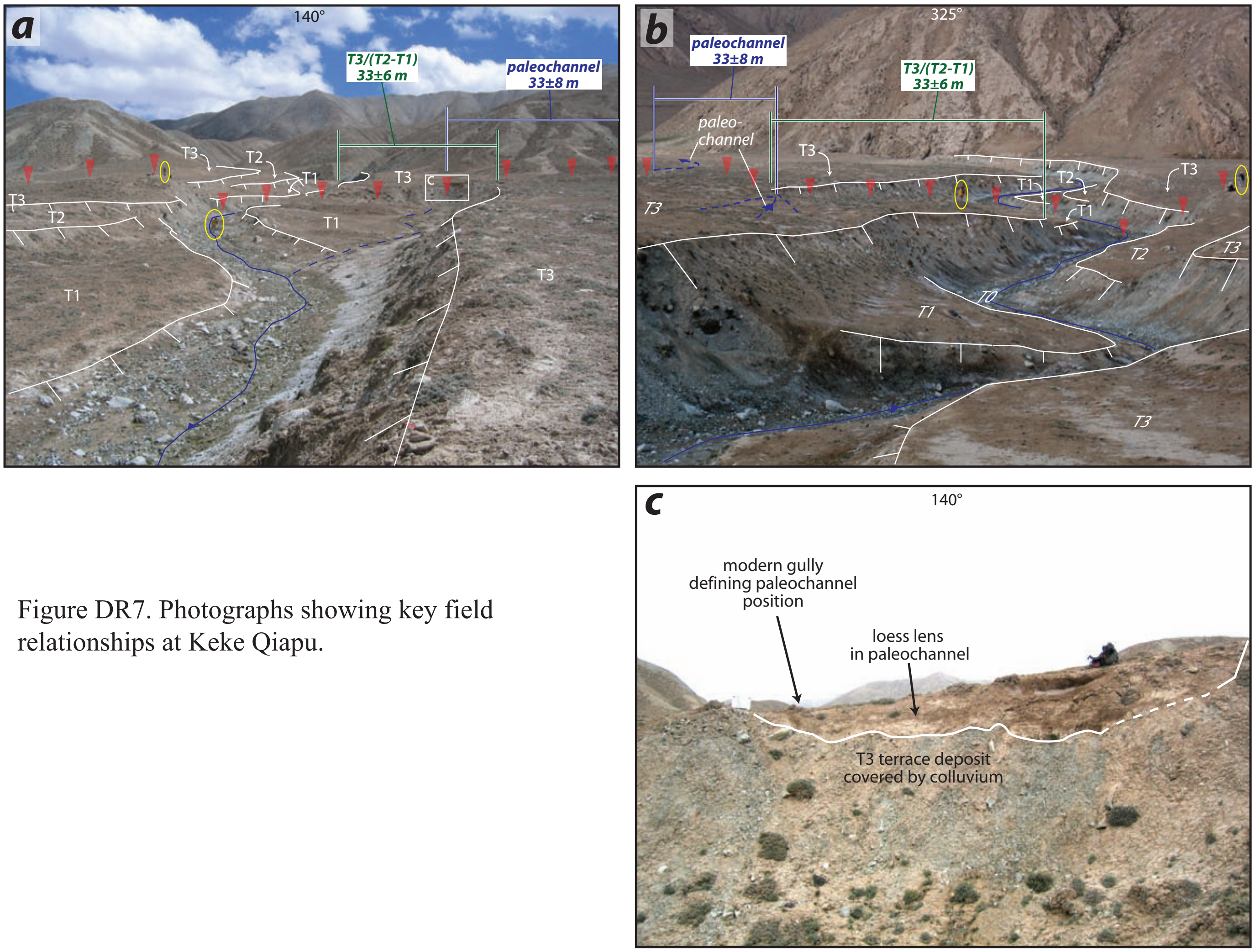

Figure DR7. Photographs showing key field relationships at Keke Qiapu.

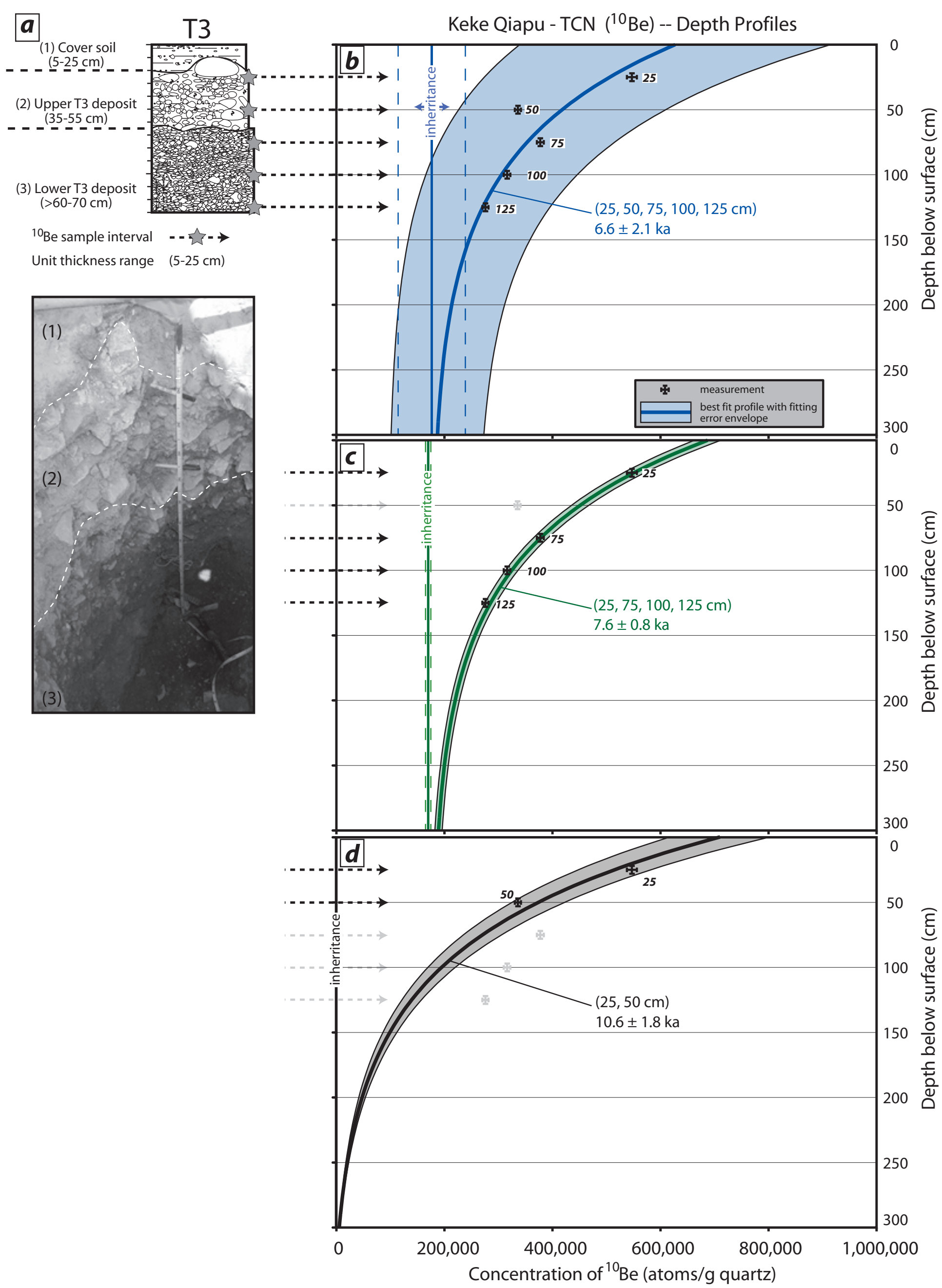

Figure DR8. T3 stratigraphy and 10Be geochronology at Keke Qiapu.

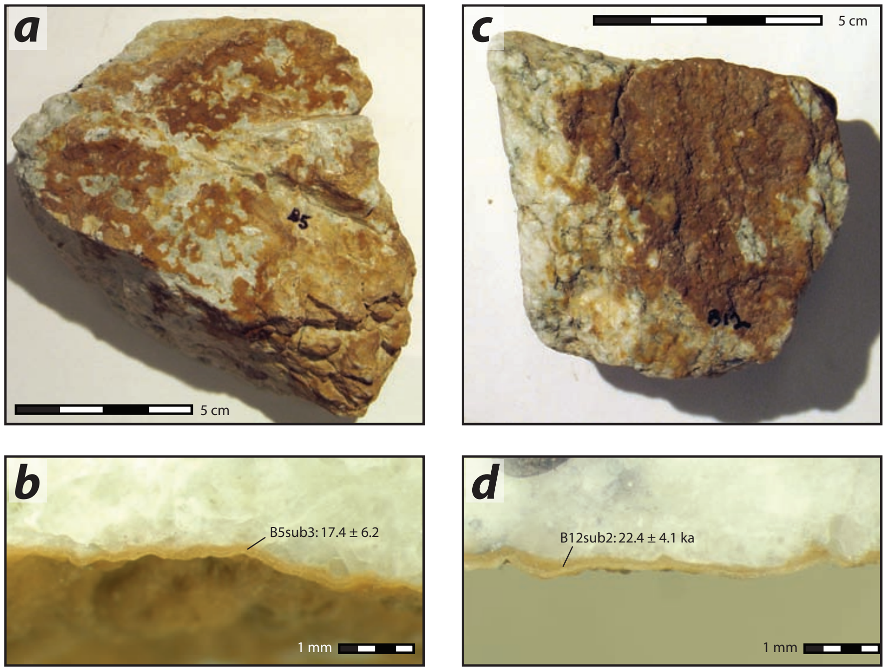

Figure DR9. Photographs of carbonate rinds analyzed in U-Series analyses.

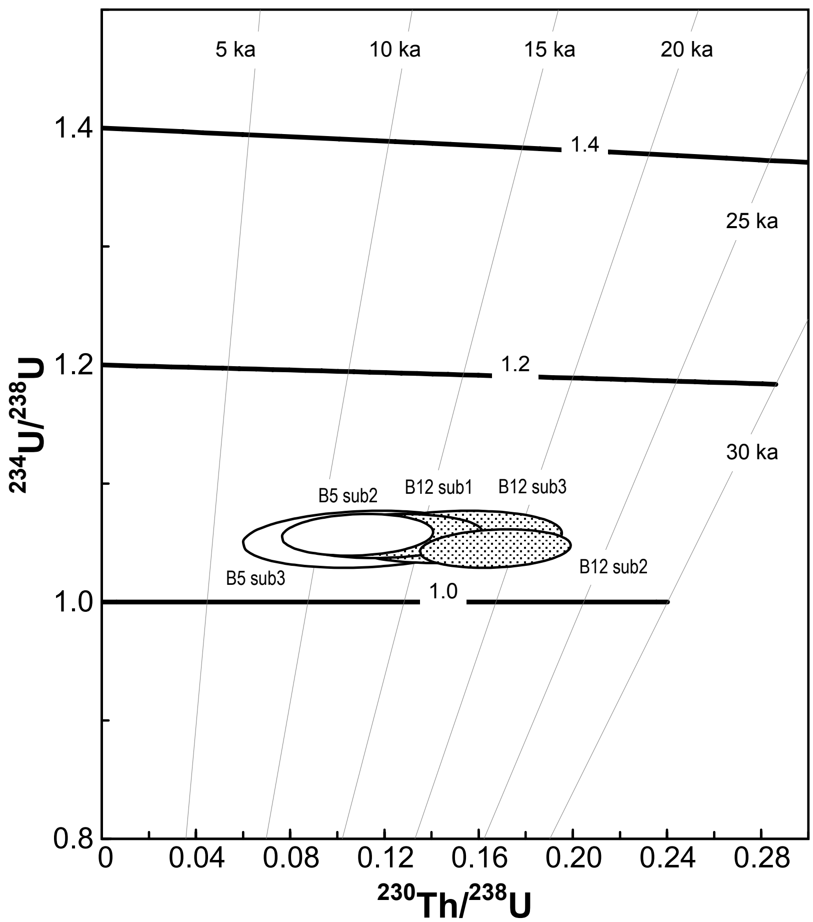

Figure DR10. Results for U-series analyses.

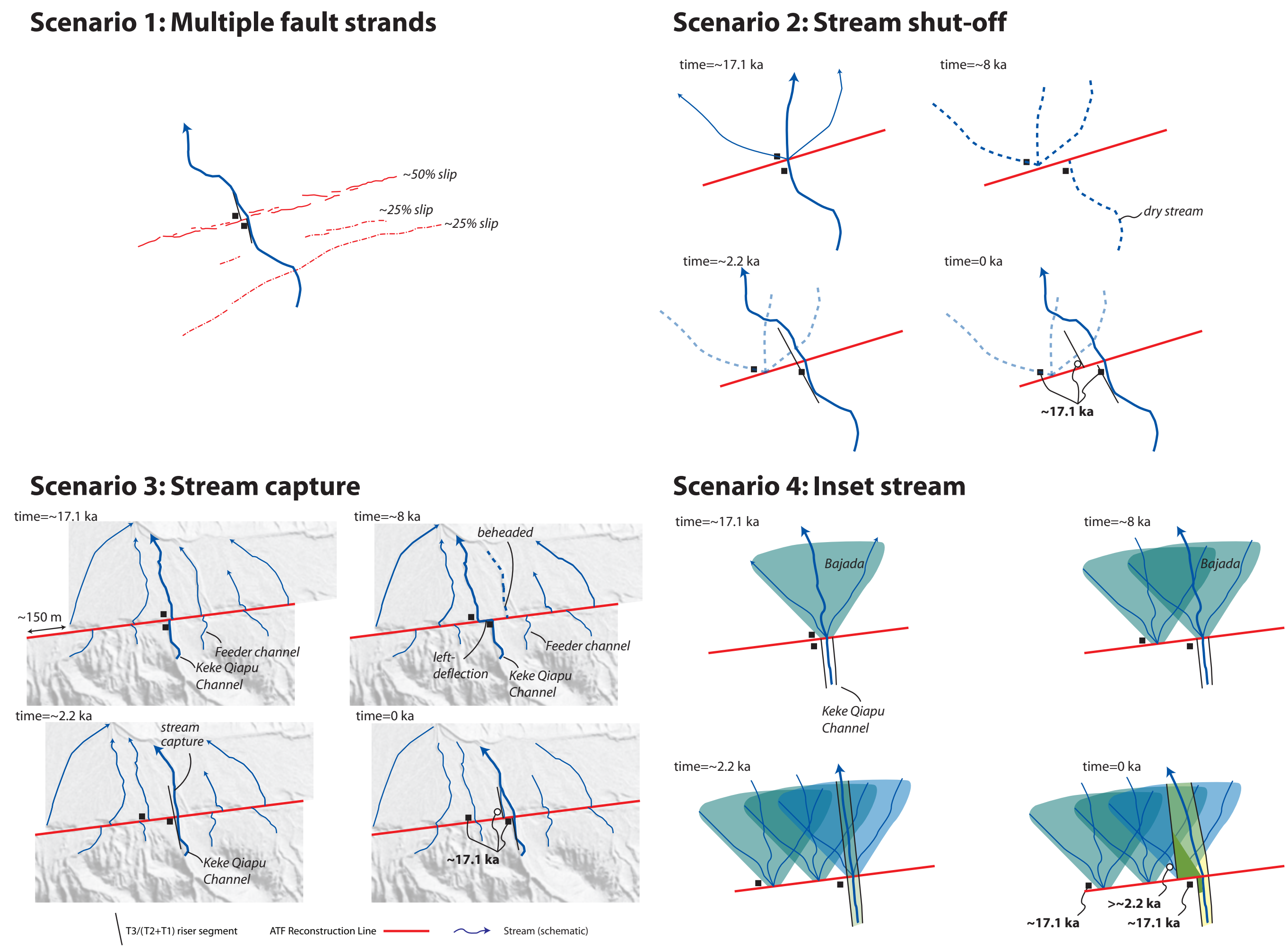

Figure DR11. Four possible reconstructions for the Keke Qiapu site.

Sample ID	UCI AMS #	Depth relative to tread (cm)[1]	Trench	Stratigraphic context	Material[2]	Fraction Modern	±	$D^{14}C$	±	^{14}C age (years BP)	±	Calibrated Age Range (calBP)[3]	
												from	*to*
C-1	41272	15	T1NE-A	colluvial gravel wedge	Animal fur	0.6817	0.0013	-318.3	1.3	3080	15	3360	3259
C-2*	41273	30	T1NE-A	colluvial gravel wedge	Charcoal	0.0803	0.0109	-919.7	10.9	20300	1100	--	22266
C-3	41274	-20	T1NE-A	F1 fan deposit	Root	0.9867	0.0020	-13.3	2.0	110	20	266	22
C-4	41275	-10	T1NE-A	F1 fan deposit	Wood or Root	0.6463	0.0013	-353.7	1.3	3505	20	3839	3704
C-5	41276	1	T1NE-A	colluvial gravel wedge	Wood or Root	0.6322	0.0012	-367.8	1.2	3685	20	4089	3931
C-6	41277	-10	T1NE-A	F1 fan deposit	Root	0.9802	0.0030	-19.8	3.0	160	25	285	-4
C-7	41278	-10	T1NE-A	F1 fan deposit	Root	1.1836	0.0023	183.6	2.3	-1350	20	--	--
*C-8**	41279	-50	T1NE-A	F1 fan deposit	Root	0.9929	0.0134	-7.1	13.4	60	110	300	--
C-9	41280	-27	T1NE-A	F1 fan deposit	Root	1.1320	0.0022	132.0	2.2	-990	20	--	--
C-10	41281	14	T1SE-A	loess wedge F2/F1	Dung	0.6757	0.0014	-324.3	1.4	3150	20	3443	3341
C-11	41282	2	T1SE-A	loess wedge F2/F1	Wood or Root	0.6820	0.0014	-318.0	1.4	3075	20	3362	3244
C-12	41283	4	T1SE-A	loess wedge F2/F1	Wood or Root	0.6985	0.0014	-301.5	1.4	2880	20	3078	2945
C-13	41284	4	T1SE-A	loess wedge F2/F1	Wood or Root	0.6623	0.0015	-337.7	1.5	3310	20	3609	3471
C-14	35767	-17	T1SE-A	F1 fan deposit	Wood	0.6555	0.0049	-344.5	4.9	3390	70	3830	3472
C-15	32088	-18	T1SE-A	F1 fan deposit	Wood	0.6686	0.0011	-331.4	1.1	3235	15	3478	3400
C-16	32089	-21	T1SE-A	F1 fan deposit	Wood	0.6752	0.0011	-324.8	1.1	3155	15	3441	3355
C-17	41285	-25	T2NE-A	F2 fan deposit	Wood or Root	0.6323	0.0015	-367.7	1.5	3680	20	4087	3929
C-18	41286	-29	T2NE-A	F2 fan deposit	Wood or Root	0.5893	0.0023	-410.7	2.3	4250	35	4870	4650
C-19	41287	-49	T2NE-A	F2 fan deposit	Wood	0.4925	0.0015	-507.5	1.5	5690	25	6535	6407
C-20	41288	-60	T2NE-A	F2 fan deposit	Wood or Root	0.5382	0.0033	-461.8	3.3	4975	50	5891	5600
C-21	41289	-62	T2NE-A	F2 fan deposit	Wood or Root	0.9759	0.0020	-24.1	2.0	195	20	294	-5
C-22	41290	30	T2NE-B	loess wedge F3/F2	Wood	0.5251	0.0015	-474.9	1.5	5175	25	5990	5903
C-23	41328	-4	T2NE-B	F2 fan deposit	Wood	0.5137	0.0012	-486.3	1.2	5350	20	6267	6005
C-24	41329	43	T2NE-B	loess wedge F3/F2	Wood	0.5452	0.0012	-454.8	1.2	4875	20	5645	5587
C-25	41306	11	T2NE-B	loess wedge F3/F2	Wood or Root	0.5090	0.0012	-491.0	1.2	5425	20	6286	6200
C-26	41307	30	T2NE-B	loess wedge F3/F2	Wood	0.5223	0.0011	-477.7	1.1	5215	20	5994	5922
C-27	41308	13	T2NE-B	loess wedge F3/F2	Wood	0.5153	0.0022	-484.7	2.2	5325	35	6259	5994
C-28	41309	31.5	T2NE-B	colluvial gravel wedge	Wood or Root	0.5131	0.0010	-486.9	1.0	5360	20	6273	6015
C-29	41310	-5	T2NE-B	F2 fan deposit	Wood or Root	0.5120	0.0013	-488.0	1.3	5380	20	6279	6030
C-30	41311	-10	T2NE-B	F2 fan deposit	Wood or Root	0.5129	0.0010	-487.1	1.0	5365	20	6275	6017
C-31	41312	-30	T2NE-B	F2 fan deposit	Wood or Root	0.5159	0.0010	-484.1	1.0	5315	20	6183	6001
C-32	35768	-12	T2SE-A	F2 fan deposit	Wood	0.5193	0.0010	-480.7	1.0	5265	20	6178	5940

C-33†	35769	-13	T2SE-A	F2 fan deposit	Wood	0.5385	0.0011	-461.5	1.1	4975	20	5744	5651
C-34†	35770	-13	T2SE-A	F2 fan deposit	Wood	0.5381	0.0010	-461.9	1.0	4980	15	5737	5657
<u>C-35</u>	35771	-22	T2SE-A	F2 fan deposit	Charcoal	0.0403	0.0072	-959.7	7.2	25800	1500	29743	23167
C-36	32090	-32	T2SE-A	F2 fan deposit	Wood	0.5161	0.0014	-483.9	1.4	5315	25	6183	6000
C-37	35772	-41	T2SE-A	F2 fan deposit	Wood	0.5360	0.0011	-464.0	1.1	5010	20	5882	5660
C-38	35773	32	T2SE-B	loess wedge F3/F2	Root	0.7602	0.0013	-239.8	1.3	2205	15	2310	2151
C-39	41313	25	T2SE-B	loess wedge F3/F2	Root	0.7780	0.0016	-222.0	1.6	2015	20	2003	1898
C-40	32091	13.5	T2SE-B	loess wedge F3/F2	Root	0.8025	0.0012	-197.5	1.2	1765	15	1720	1615
C-41	32092	2	T2SE-B	loess wedge F3/F2	Root	0.8628	0.0017	-137.2	1.7	1185	20	1174	1059
C-42	41314	19	T2SE-B	loess wedge F3/F2	Root	0.8014	0.0015	-198.6	1.5	1780	20	1811	1619
C-43	41315	2	T2SE-B	loess wedge F3/F2	Wood or Root	0.5736	0.0011	-426.4	1.1	4465	20	5280	4976
C-44	41316	0	T2SE-B	F2 fan deposit	Wood or Root	0.5345	0.0023	-465.5	2.3	5030	35	5895	5662
C-45	41317	-26	T2SE-B	F2 fan deposit	Wood or Root	0.5627	0.0018	-437.3	1.8	4620	30	5462	5297
C-46	41318	-23	T2SE-B	F2 fan deposit	Wood or Root	0.5200	0.0011	-480.0	1.1	5255	20	6175	5935
C-47	41319	-13	T3NE-A	upper F3 fan deposit	Wood or Root	0.4845	0.0011	-515.5	1.1	5820	20	6715	6554
<u>C-48</u>	41320	-50	T3NE-A	upper F3 fan deposit	Wood or Root	0.2161	0.0066	-783.9	6.6	12310	250	15119	13733
<u>C-49</u>	41321	-52	T3NE-A	upper F3 fan deposit	Wood or Root	0.4006	0.0016	-599.4	1.6	7350	35	8303	8030
<u>C-50</u>	41322	-58	T3NE-A	lower F3 fan deposit	Wood or Root	0.3058	0.0093	-694.2	9.3	9520	250	11616	10203
C-51	41323	-18	T3SE-A	upper F3 fan deposit	Wood or Root	0.5395	0.0011	-460.5	1.1	4955	20	5731	5612
C-52	41324	-46	T3SE-A	upper F3 fan deposit	Root	0.5095	0.0014	-490.5	1.4	5415	25	6284	6188

[1]Positive value indicates above tread; negative value indicates below tread.

[2]Material as interpreted in the field and through examination under microscope.

[3]Ages calibrated using InterCal04 (Reimer et al., 2004) and OxCal v.4.0.1 software (Bronk Ramsey, 1995; 2001). Age range is reported at the 2-sigma (2-σ) confidence interval.

gray italics indicates modern sample

<u>underlined</u> indicates detrital sample

*Calibrated age range could not be calculated based on currently available calibration curve.

†Sample with replicate analyses.

Table DR1. ^{14}C AMS analyses from Kelutelage.

Sample ID	UCI AMS #	Depth relative to tread (cm)[1]	Trench	Stratigraphic context	Material[2]	Fraction Modern	±	$D^{14}C$	±	^{14}C age (years BP)	±	Calibrated Age Range (calBP)[3] from	to
C-53	35732	11	T1SE-A	loess wedge at base of T2/T1 riser	wood	0.6326	0.0017	-367.4	1.7	3680	25	4090	3925
C-54	35733	8	T1SE-A	loess wedge at base of T2/T1 riser	wood	0.6464	0.0017	-353.6	1.7	3505	25	3845	3697
C-55	32082	7	T1SE-A	loess wedge at base of T2/T1 riser	wood	0.6343	0.0010	-365.7	1.0	3655	15	4077	3908
C-56	35734	-4	T2NE-A	T2 strath	wood	0.6230	0.0012	-377.0	1.2	3800	20	4242	4095
C-57	35738	-6	T2NE-A	T2 strath	wood	0.6271	0.0011	-372.9	1.1	3750	15	4213	4006
C-58	35739	-21	T2NE-A	old alluvium	wood or root	0.5376	0.0050	-462.4	5.0	4990	80	5903	5599
C-59	32101	-35	T2NE-A	old alluvium	charcoal	0.0161	0.0015	-983.9	1.5	33170	780	34920	31735
C-60	35753	25	T2SE-A	loess wedge at base of T3/T2 riser	charcoal	0.5068	0.0031	-493.2	3.1	5460	50	6397	6126
C-61	32102	4	T2SE-A	loess wedge at base of T3/T2 riser	charcoal	0.5592	0.0019	-440.8	1.9	4670	30	5569	5316
C-62	35754	-7	T2SE-B	T2 strath	charcoal	0.5730	0.0010	-427.0	1.0	4475	15	5283	4987
C-63	35755	-16.5	T2SE-B	old alluvium	charcoal	0.0278	0.0031	-972.2	3.1	28770	890	30808	27146
C-64	35756	-30	T2SE-B	old alluvium	charcoal	0.0063	0.0010	-993.7	1.0	40800	1300	44047	38495
C-65	32113	-34	T2SE-B	old alluvium	charcoal	0.0133	0.0021	-986.7	2.1	34700	1300	37947	32395
C-66	32083	14	T3NE-A	loess wedge at base of T4/T3 riser	charcoal	0.7678	0.0012	-232.2	1.2	2125	15	2153	2010
C-67	35757	12	T3NE-A	loess wedge at base of T4/T3 riser	charcoal	0.3462	0.0031	-653.8	3.1	8520	80	9683	9318
C-68	35758	2	T3NE-B	soil	wood	0.4999	0.0009	-500.1	0.9	5570	20	6401	6306
C-69	35759	-9	T3NE-B	old alluvium	charcoal	0.0174	0.0028	-982.6	2.8	32500	1300	35747	30195
C-70	32084	-28.5	T3NE-B	old alluvium	charcoal	0.0081	0.0011	-991.9	1.1	38700	1100	41326	36725
C-71	32114	38	T3SE-A	loess wedge at base of T4/T3 riser	charcoal	0.6073	0.0137	-392.7	13.7	4010	190	5030	3927
C-72	35760	3	T3SE-A	colluvial gravel at base of T4/T3 riser	charcoal	0.0129	0.0036	-987.1	3.6	34900	2200	42162	31150
C-73*	35761	-38	T3SE-A	old alluvium	charcoal	0.0011	0.0016	-998.9	1.6	>43800	--	--	--
C-74	32085	-17	T3SE-B	old alluvium	charcoal	0.0168	0.0011	-983.2	1.1	32820	550	34007	31787
C-75	35762	-10	T3SW-A	T3 strath	wood or root	0.7733	0.0014	-226.7	1.4	2065	15	2112	1989
C-76	32086	-24	T3SW-A	old alluvium	wood or root	0.7705	0.0014	-229.5	1.4	2095	15	2120	2002
C-77	35763	-26	T3SW-A	old alluvium	charcoal	0.0402	0.0088	-959.8	8.8	25800	1900	31436	22521
C-78	32087	-50	T3SW-A	old alluvium	wood or root	0.8492	0.0014	-150.8	1.4	1315	15	1292	1184
C-79	35764	-52	T4NE-A	old alluvium	charcoal	0.0040	0.0016	-996.0	1.6	44300	3100	58350	39463

C-80*	32115	5	T4SE-A	soil	charcoal	0.0743	0.0041	-925.7	4.1	20880	450	24163	--
C-81	32116	-6	T4SE-A	T4 strath	charcoal	0.0232	0.0016	-976.8	1.6	30250	570	31485	29180
C-82	35765	-32	T4SE-A	old alluvium	charcoal	0.0066	0.0016	-993.4	1.6	40400	1900	46036	37121
C-83	35766	-6	T4SW-A	soil	wood or root	0.8962	0.0025	-103.8	2.5	880	25	905	731
C-84	32117	-13	T4SW-A	soil	wood or root	0.7350	0.0056	-265.0	5.6	2470	70	2724	2357
C-85	32118	-42	T4SW-A	old alluvium	charcoal	0.0069	0.0016	-993.1	1.6	39900	1800	45068	36781

[1]Positive value indicates above tread; negative value indicates below tread

[2]Material as interpreted in the field and through examination under microscope.

[3]Ages calibrated using InterCal04 (Reimer et al., 2004) and OxCal v.4.0.1 software (Bronk Ramsey, 1995; 2001). Age range is reported at the 2-sigma (2-σ) confidence interval.

underlined indicates pre-Holocene sample associated with deposition old alluvium

*Calibrated age range could not be calculated based on currently available calibration curve.

Table DR2. ^{14}C AMS analyses from Yukuang.

Sample Name[2]	Wt	U	^{232}Th	$^{230}Th/^{232}Th$	$^{230}Th/^{238}U$	2-σ	$^{234}U/^{238}U$	2-σ	Age[3]	2-σ
	(mg)	(ppm)	(ppm)			(% error)		(% error)	(ka)	(absolute)
B5 sub1	8.22	7.442	4.401	1.0	0.1890	4.9	1.0478	0.5	3.3	±11.3
B5 sub2	8.63	7.232	1.217	2.8	0.1542	1.8	1.0509	0.7	12.4	±2.9
B5 sub3	12.38	6.306	1.637	2.1	0.1783	2.0	1.0454	0.4	12.7	±4.5
B12 sub1	11.77	7.095	1.485	2.6	0.1766	2.6	1.0445	0.3	14.0	±3.6
B12 sub2	11.77	8.038	1.374	3.7	0.2080	2.8	1.0386	0.5	19.3	±3.0
B12 sub3	11.15	6.078	1.428	2.7	0.2062	5.2	1.0435	0.6	17.0	±4.3

[1] Isotope ratios are activity ratios.

[2] Samples are designated by clast number, followed by sub sample (e.g., "B5 sub1" indicates the first sub sample measured on clast B5).

[3] Correction for initial ^{230}Th was made assuming $^{232}Th/^{238}U = 1.2 \pm 0.5$, $^{230}Th/^{238}U = 1.0 \pm 0.25$, and $^{234}U/^{238}U = 1.0 \pm 0.25$. Decay constants are those of Cheng et al (2000).

Table DR3. $^{230}Th/U$ geochronology at Keke Qiapu.

Dal-CNEF ID	Sample Name	Latitude[1]	Longitude[1]	Altitude[1]	Site Surface Production Rate[2]	Depth[3]	Number of clasts[4]	Subsurface production rate[5,6]	Quartz mass	Mass carrier solution[7]	$^{10}Be/^{9}Be$	$^{10}Be/^{9}Be$	^{10}Be concentration	±[9]
		(°N)	(°E)	(km)	(atoms/g/yr)	(cm)	(n)	(atoms/g/yr)	(g)	(g)	Corrected for Blank & Boron[8]	Error	(10^6 atoms/g SiO_2)	
2085	Blank for 20080723	--	--	--	--	--	--	--	0	0.2332	5.295E-15	5.612E-16	--	--
2146	05S3T5SW-25	38.081436	88.166298	4023	68.28	25	53	49.294	70.7781	0.2407	2.402E-12	4.044E-14	546913	9209
2147	05S3T5SW-50	38.081436	88.166298	4023	68.28	50	53	35.676	93.9987	0.236	1.998E-12	3.379E-14	335898	5681
2148	05S3T5SW-75	38.081436	88.166298	4023	68.28	75	118	25.905	95.435	0.2283	2.357E-12	3.970E-14	377511	6359
2149	05S3T5SW-100	38.081436	88.166298	4023	68.28	100	92	18.890	89.8601	0.227	1.868E-12	3.601E-14	315962	6091
2150	05S3T5SW-125	38.081436	88.166298	4023	68.28	125	62	13.852	89.8185	0.2392	1.547E-12	3.141E-14	275949	5601

[1] Latitude, longitude, and altitude determined from handheld GPS unit.

[2] Surface production rate calculated using CRONUS ^{10}Be / ^{26}Al exposure age calculator, v.2 (Balco et al., 2008).

[3] Depth measured to the middle of stratigraphic interval from which clasts were collected. Samples were collected from intervals ~6 cm thick.

[4] Clasts were amalgamated following the technique of Anderson (1996), Repka et al. (1997), and Hancock et al. (1999). Quartz content of all samples estimated at >15% from hand sample.

[5] The following values were used for the production rate calculation: $\Lambda = 160$ g/cm^2; $\rho = 2$ g/cm^3 for overlying deposit; $\rho = 2$ g/cm^3 for clasts; $\lambda = \ln(2)/1360000$.

[6] Surface geometry was assumed to be horizontal and no corrections were made for snow cover, erosion, or horizon topographic obstructions (negligible).

[7] Carrier concentration 1015 μg/ml and carrier density 1.013 g/ml.

[8] Blank correction made using Dal-CNEF 2085.

[9] Concentration error (1-σ) includes propagation of the uncertainties in the blank, carrier, and counting statistics.

Table DR4. Keke Qiapu ^{10}Be geochronology.